THE
PHYSICAL REVIEW

A journal of experimental and theoretical physics established by E. L. Nichols in 1893

SECOND SERIES, VOL. 174, NO. 4 20 OCTOBER 1968

Double Charge Exchange of Positive π Mesons on Complex Nuclei*

P. E. BOYNTON, THOMAS J. DEVLIN,† AND J. SOLOMON‡
Princeton-Pennsylvania Accelerator and Palmer Physical Laboratory, Princeton University, Princeton, New Jersey 08540

AND

V. PEREZ-MENDEZ
Lawrence Radiation Laboratory, University of California, Berkeley, California 94720

(Received 15 April 1968)

The differential cross section for the reaction $\pi^+ + N(z,n) \rightarrow \pi^- + X$ was measured at lab angles 8.5° and 16°, with incident 200-MeV π^+ mesons. Several target nuclei were employed: V^{51}, Zr^{90}, and Li^7. The momentum analysis of the final-state π^- was accomplished with a magnetic spectrometer, using digitized wire spark chambers for track location. Recent theoretical papers indicate the possiblity of exciting isobaric analog states [for which $X = N(z+2, n-2)$: a two-body final state]. Our data show no evidence of this state, and provide an upper limit of 1–2 μb/sr on its excitation at both 8.5° and 16°. The contribution to the cross section from all final states is 40–60 μb/sr for the various targets and angles and for $110 \geq T_{\pi^-} \geq 200$ MeV. The data are discussed in terms of a pion-complex-nucleus interaction model, including effects of higher-order inelastic scattering.

INTRODUCTION

OVER the past five years, several authors[1–3] have pointed out that π mesons may be useful probes of nuclear structure and have urged experimental and theoretical participation in the study of pion-nucleus scattering. Recently, extensive proton scattering work[4] involving *single* isobaric analog states (IAS) ($\Delta t_z = 1$) has yielded much information on Coulomb displacement energies, isospin selection rules, and level structure for a broad range of nuclear mass. These findings lead to consideration of extending such measurements to higher nuclear isospin multiplets through double-charge-exchange (DCX) processes.[5] This experiment was then motivated by the possibility of exciting $\Delta t_z = 2$ IAS in target nuclei via the pion DCX reaction

$$\pi^+ + N(z,n) \rightarrow N(z-2, n+2) + \pi^- . \qquad (1)$$

These previously inaccessible *double* analog states should provide additional information on nuclear structure by an extension of these studies further off the line of stable nuclides.

The existence of DCX reactions was first observed experimentally by Batusov *et al.*[6] They measured the total cross section for this process on emulsion nuclei. Two other experiments were carried out prior to our own. Gilly *et al.*[7] measured the DCX π^- energy spectrum from $T = \frac{1}{2}$ ground-state nuclei (Li^7, Be^9, and Na^{23}) at 0° scattering angle. Their results for Li^7 showed a peak in the spectrum which they tentatively identified with a two-body final state. Davis *et al.*[8] measured the DCX cross section for π^- on copper at a scattering angle of 90°. Neither of these experiments included the possibility of observing double-analog-state transitions, the

* Work supported in part by the U. S. Atomic Energy Commission under Contract No. AT(30-1)-2137.

† Present address: Physics Department, Rutgers—The State University, New Brunswick, N. J.

‡ Present address: Physics Department, University of Illinois at Chicago Circle, Chicago, Ill.

[1] T. Ericson, in Proceedings of the CERN 1963 Conference on High-Energy Physics and Nuclear Structure (unpublished).

[2] S. Drell and A. De Shalit (private communication), quoted by T. Ericson, in Proceedings of the CERN 1963 Conference on High-Energy Physics and Nuclear Structure (unpublished).

[3] M. Jean, Nuovo Cimento Suppl. **2**, 400 (1964).

[4] *Isobaric Spin in Nuclear Physics*, edited by J. Fox and D. Robson (Academic Press Inc., New York, 1966).

[5] G. T. Garvey, J. Cerny, and R. H. Pehl, Phys. Rev. Letters **12**, 726 (1964); C. J. Batty, E. Friedman, and P. C. Rowe, Phys. Letters **19**, 33 (1965).

[6] Yu. Batusov *et al.*, Yadern Fiz. **3**, 309 (1966) [English transl.: Soviet J. Nucl. Phys. **3**, 223 (1966)].

[7] L. Gilly *et al.*, Phys. Letters **11**, 224 (1964).

[8] R. Davis *et al.*, Bull. Am. Phys. Soc. **9**, 627 (1964).

former because of choice of nuclei, and the latter because of projectile charge state.

The experiment described in this paper was the first to search for double-analog-state transitions. The work was reported in preliminary form in Ref. 9. Subsequent work by Cook *et al.*[10] has also been directed toward the study of double analog states. At the time of their report, they placed an upper limit of 4 μb/sr (at 30°) on the production of the double analog state by 30-MeV π^+ on vanadium.[10a]

Because of the prospect of low cross sections generally associated with double scattering processes, and specifically predicted for reaction (1), this experiment was planned to take advantage of the peak in the elementary pion-nucleon cross section at the 3,3 resonance (190-MeV incident pions). Several theoretical papers have treated the pion DCX reaction near this energy.[11–13] Of particular relevance to our experiment is the work of Brown and Barshay, which assumes the charge exchange to proceed through two intermediate 3,3 isobars. When isobar recoil is taken into consideration, the cross section is found to be roughly a factor of 10 lower than when calculated in the static limit (no recoil). Brown and Barshay also point out a marked enhancement of the cross section resulting from the collective nature of the $\Delta t_z=2$ transitions in nuclei with neutron excess. For the case in which there are only neutrons in the unfilled shell, the cross section is proportional to the number of neutron pairs. As a crude numerical estimate based on their results for Ca^{48}, we write (at 0°)

$$d\sigma/d\Omega=\Delta n(\Delta n-1)\times 4\ \mu\text{b/sr}, \tag{2}$$

where Δn is the neutron excess. This value is reduced by roughly a factor of 2 at 15°.

Ca^{48} and Zr^{90} are obvious choices for collective neutron-pair enhancement of the cross section. However, because a sufficient amount of those isotopes was not available, natural-isotopic-abundance targets of zirconium and vanadium were used. A light target, lithium, was included to provide overlap with the measurements of the CERN group (Gilly *et al.*).

DCX scattering to nonanalog states and the continuum is anticipated. However, for our targets the Q value for the IAS transition Q_{IAS}, is necessarily less than for any other reaction. Thus for a zero-energy-width incident π^+ beam the final-state π^- energy spectrum should be characterized by a narrow peak (<0.2 MeV wide[14]) displaced by Q_{IAS} from the incident beam energy, followed on the low-energy side by an increasing inelastic component.

Observation of this peak was the primary concern of the experiment. In order to identify possible IAS transitions, the Q values for DCX interactions in the relevant targets were calculated. Since actual measurements of the Coulomb energy displacement E_c associated with the single IAS of V^{51} and Zr^{90} already existed, the additional increment E_c' (the Coulomb energy difference between *single* and *double* analogs) was computed in terms of E_c using a charged-sphere model:

$$E_c=(6e^2/5R)(z+\tfrac{1}{2}); \tag{3}$$

then

$$E_c'=E_c\frac{z+\frac{3}{2}}{z+\frac{1}{2}}, \tag{4}$$

and it follows that

$$Q_{\text{IAS}}=-E_c\left(1+\frac{z+\frac{3}{2}}{z+\frac{1}{2}}\right)+2\delta, \tag{5}$$

where δ is the n-H mass difference. Numerical results, along with other target data, are shown in Table I.

EXPERIMENTAL METHOD

Positive π mesons were produced by focusing the 740-MeV external proton beam of the University of California Lawrence Radiation Laboratory 184-in. synchrocyclotron onto a polyethylene target. The over-all layout of the proton and pion beams is shown in Fig. 1. The triple-focus pion beam was designed to minimize flight path while getting the beam out of the high-background-radiation environment of the proton cave and into the adjacent experimental area. At maximum proton beam intensity the rate of 300-MeV/c π^+ at the final target position (2×2-in. spot) was 6×10^4/sec. The muon and electron contaminations of the beam were determined by range measurements and a gas Čerenkov counter to be (13±1) and (2.6±0.2)%, respectively.

Protons were removed by differential energy loss in a CH_2 absorber at the momentum slit and subsequent sweeping from the beam by the second bending magnet. A small residual proton component at the DCX target was eliminated by time-of-flight methods.

TABLE I. Target specifications.

Dominant isotope	Q value (MeV)	Shell structure p	Shell structure n	Target thickness (g/cm²)
Zr^{90} (51.5%)	−25.4±1	$(2p_{1/2})^8$	$(1g_{9/2})^{10}$	8.06
V^{51} (99.7%)	−18.0±1	$(1f_{7/2})^3$	$(1f_{7/2})^8$	6.05
Li^7 (92.5%)	···	$(1p_{3/2})^1$	$(1p_{3/2})^2$	2.03

[9] P. Boynton, J. Solomon, T. Devlin, and V. Perez-Mendez, Bull. Am. Phys. Soc. **11**, 37 (1966).

[10] C. Cook, R. Burman, and M. Nordburg, Bull. Am. Phys. Soc. **12**, 104 (1967).

[10a] *Note added in proof.* We have received a final report by these authors [University of Rochester Report No. UR-875-237 (unpublished)] which indicates a cross-section upper limit of approximately 1 μb/sr [C. Cook *et al.*, Phys. Rev. (to be published)].

[11] G. E. Brown and S. Barshay, Phys. Letters **16**, 165 (1965).

[12] R. G. Parsons, J. S. Trefil, and S. D. Drell, Phys. Rev. **138**, B847 (1965).

[13] F. Becker and Z. Maric, Nuovo Cimento **36**, 1395 (1965).

[14] J. D. Anderson, C. Wong, and J. W. McClure, Phys. Rev. **126**, 2170 (1962).

The entire complex of equipment shown in Fig. 2 which detected the final-state pion will be referred to as the "spectrometer." The design was guided by considerations of momentum resolution, data-handling efficiency, and background rejection. Each of these points is discussed in following paragraphs.

An incident pion was defined by the coincidence $B_1B_2B_3$, where, for example, B_1 is any one of the triplet of counters B_{1a}, B_{1b}, and B_{1c} of Fig. 2. The counters A_1 in the pion beam downstream from the DCX target were placed in anticoincidence and served to define a pion which interacted in the target. The coincidence S_1, S_2, S_3, S_4, and S_5 defined a negatively charged particle which passed through the spectrometer. A_2 was placed in anticoincidence to negate pole-tip scattering in the magnet. The anticoincidence counter A_3 was placed in the path of all positively charged particles which entered the spectrometer and eliminated their contribution to the accidental trigger rate. The Čerenkov counter placed in anticoincidence served to eliminate electrons. The entire coincidence logic $B_1B_2B_3\bar{A}_1\bar{A}_2\bar{A}_3\bar{C}S_1S_2S_3S_4S_5$ identified a DCX event.

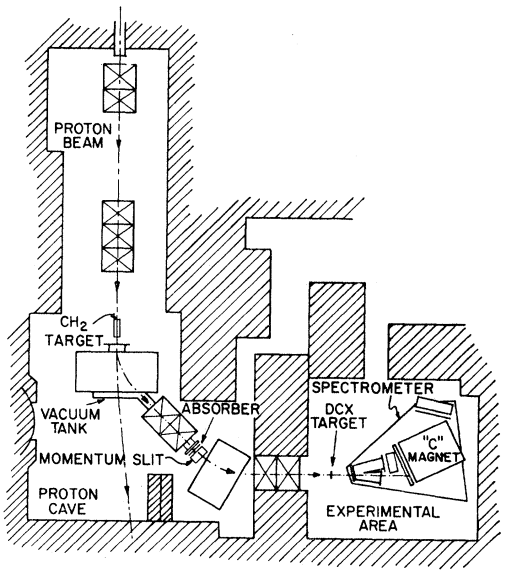

FIG. 1. Plan view of general experimental layout at the 184-in. cyclotron.

The spectrometer employed a 16×36-in. C magnet with an 8-in. gap and 15 000-G central field. The broad range of bending angles afforded by a 90° sector magnet enabled momentum analysis from 180 to 340 MeV/c with a single field setting. Canting the poleface at 20° with respect to the central scattered ray provided vertical-focusing characteristics which roughly optimized the aperture and the solid angle. Over most of the momentum range of interest in the experiment, scintillator S_3 at the entrance to the magnet gap defined the solid angle (see Fig. 2). The exit scintillators S_4 and S_5 limited the solid angle only at the lowest momenta. Below 210 MeV/c trajectories intersecting S_3 begin to fall short of the low-momentum edge of S_4-S_5. This critical point depends on the horizontal dimensions of S_3 and S_4-S_5. Constancy of detector solid angle for higher momenta depends on the vertical extent of these counters. Wire-orbit techniques were used to determine the appropriate shape for S_3 such that all trajectories through S_3 remain within the magnet aperture. This momentum dependence of detector solid angle was verified by the data themselves through the correlation between momentum and horizontal position of trajectories at S_3. Such measurements were completely consistent with a straightforward Monte Carlo simulation of this momentum dependence shown in Fig. 3. All methods indicate that the solid angle (geometric efficiency) is constant between 210 and 330 MeV/c. The consequent trapezoidal shape of S_3 (see Fig. 2) results in a known angular sampling bias with mean value of about +1° at both 7.5° and 15° scattering-arm

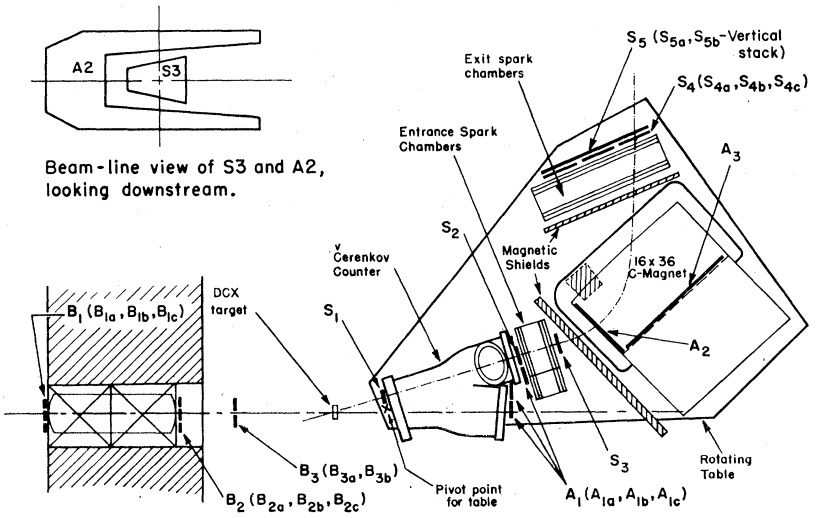

FIG. 2. Schematic detail of beam-defining counters and spectrometer. In the text, B refers to the coincidence B_1, B_2, B_3 and S to S_1, S_2, S_3. Coincidence $B_1B_2B_3S_1\bar{C}S_2S_3\bar{A}_1\bar{A}_2\bar{A}_3S_4S_5$ defines a DCX event.

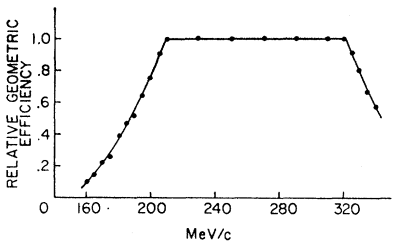

FIG. 3. Results of Monte Carlo calculation of the momentum dependence of spectrometer geometric detection efficiency. Momentum scale refers to values within C magnet; energy loss in spectrometer and targets is ~20 MeV for V and Zr.

positions. Hereafter these mean-sampled angles of 8.5° and 16° are referred to simply as scattering angles.

Momentum Resolution

Success in observing a two-body final-state "peak" in the momentum spectrum depends on the signal-to-noise ratio determined by experimental resolving power and backgrounds arising from other processes. The spectrometer was designed for 1% momentum resolution. To check this parameter, the momentum-defining slit (Fig. 2) was calibrated during the beam-tuning procedure and a pion beam [≥4-MeV full width at half-maximum (FWHM)] was directed into the spectrometer. The measured width of 6-MeV FWHM indicated a spectrometer-resolution figure consistent with 1%. The role of the energy width of the incident beam is of course as important as spectrometer resolution in measurement of the π^- spectrum. Since a 10-MeV FWHM beam was found necessary to provide reasonable counting rates, an over-all resolution full width of 10 MeV results from the dominant beam-width contribution. For resolution widths greater than the characteristic 0.2 MeV for IAS transitions, the signal-to-noise ratio arising from a background of continuum DCX transitions is roughly proportional to the width. Thus for a 1-μb/sr-MeV continuum background and a 10-μb/sr IAS peak, the signal-to-noise ratio is approximately unity for a 10-MeV resolution width. It will be seen later that the background in the vicinity of the IAS channel was in fact substantially less than 1 μb/sr MeV for both vanadium and zirconium. Thus double-analog-state transition cross sections consistent with the Brown-Barshay model (100–200 μb/sr) would have been easily observed.

Electronics

The fast electronics circuitry block-diagrammed in Fig. 4 was constructed with Chronetics logic modules; the resolving time at each stage in the logic is indicated roughly by the output pulse rates of the preceding modules. Amperex 56AVP photomultiplier tubes were used throughout except for the low-rate counters S_3, A_2, S_4, and S_5 which were a mixture of RCA types 7746 and 6810A. The 56AVP tube-base electronics was a Zener diode buffered design developed for high-rate, moderate-gain application. The tube-base combination was tested at synchronous pulse rates to 20 MHz using a GaP diode as a light source. No noticeable decrease in gain was observed even at 20 MHz for pulse lengths and heights comparable with those encountered with scintillators. The phototube signal was direct-coupled to the output connector. Each phototube was followed by a direct-coupled limiter prior to discrimination. Particular care was taken with the high-rate veto A_1 which was used in conjunction with a direct-coupled anticoincidence.

All B and S counters were $\frac{1}{8}$-in.-thick Pilot B scintillation material, except for S_4 and S_5, which were $\frac{1}{2}$ in. thick. All anticounters were $\frac{1}{4}$ in. thick, except for A_3, which is $\frac{1}{2}$ in.

Spark Chambers

Four wire spark chambers (two gaps each) with magnetostrictive delay lines and associated analog-digital conversion electronics provided a rapid data-handling system enabling overnight computer data processing. The progress of the experiment was thereby monitored in considerable detail day by day, a particularly valuable feature from the standpoint of instrumentation diagnostics and guiding optimal use of beam time. Details of the construction and operating characteristics of these units and the associated elec-

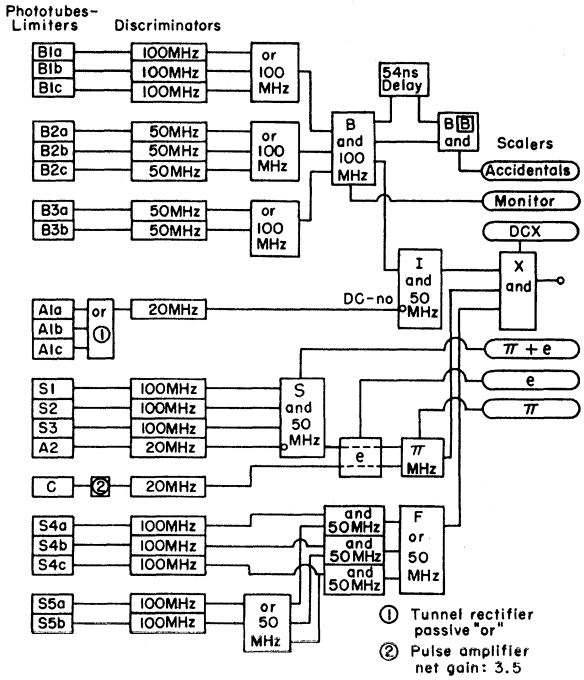

FIG. 4. Electronic logic diagram. See Fig. 2 for scintillator designations and positions.

TABLE II. Spark-chamber specifications.

	Entrance chambers		Exit chambers
Number of gaps	4		4
Gap size		0.375 in.	
Chamber spacing[a]		8.0 in.	
Wire count		24/in.	
		6-mil aluminum wire	
Over-all wire-plane dimensions	8×8 in.		18×22 in.
Active area (defined by scintillators)	4×3.5 in.		16×20 in.
Chamber mass	0.13 g/cm²		0.23 g/cm²
Operating voltage		8 kV (across 500 $\mu\mu$F)	
Gas composition		10% Ne, 90% He	
Average gap efficiency[b]	98%		97%

[a] If measured along the normal to the first wire plane, gap midplanes are located at 0.1875, 0.3750, 7.4375, and 7.8125 in.
[b] Derived from the same set of data yielding 1200 four-spark tracks mentioned in the data-analysis discussion. These average efficiencies are calculated by comparing the relative number of eight-spark tracks with seven- and six-spark tracks. The number of tracks with less than six sparks is negligible.

tronics have been reported.[15,16] A summary of specifications of these chambers is given in Table II.

The first and last wires in each wire plane were capacitively coupled to the high-voltage pulse supply and were thereby pulsed coincidently with each chamber discharge, providing a set of fiducial measurements for each spark pattern. Because of slow drifts in these values, a running average of fiducials including only the previous 10 triggers was used in computing spark coordinates for a given event. Variation in fiducial lengths over this interval seldom exceeded 0.1%.

A detailed evaluation of wire-spark-chamber spatial resolution has been carried out,[17] and the results may be briefly summarized as

$$\sigma_{ent}=0.016 \text{ in.},$$
$$\sigma_{ex}=0.019 \text{ in.}$$

Noted here is the standard deviation in spark coordinate measurement in a typical wire plane in both entrance and exit chambers. These values were derived from a sample of 1200 four-spark tracks and compare favorably with the half-width, ~0.21 in., of the actual wire spacing. It is assumed that the larger-angle trajectories (with respect to the normal to the chamber face) are responsible for the larger variance in the rear chamber.

Electron Background

Sources of particles indistinguishable (with a simple spectrometer) from legitimate DCX events were considered in some detail during the design phase of this experiment. The major contribution arises from single-charge-exchange scattering of pions in the DCX target and subsequent pair production by γ rays from π^0 decay.

A low-mass threshold Čerenkov counter with a propane (gas) radiator was constructed to detect and electronically reject this electron background. As shown in Fig. 5, the counter is composed of two intersecting cylinders which straddle both direct and scattered beam lines. All three windows are 25-mil pressure-formed Duraluminum. When pressurized to 6 atm of propane, the total mass along either beam line was less than 1.5 g/cm². The choice of propane as Čerenkov radiator was determined by the design goals of low mass and high detection efficiency for a given counter length (large refractive index/molecular wt).

The optical system (mirror size, orientation, and curvature) was designed by graphical ray tracing, taking into account particle-beam size and angular definition and the Čerenkov propagation angle.

The photon detection system consisted of an Amperex 58AVP 5-in. photomultiplier tube followed by a Chron-

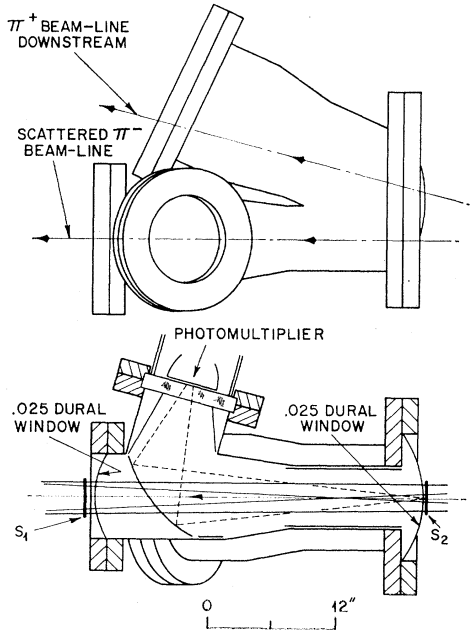

FIG. 5. Čerenkov-counter geometry, plan and elevation views. Solid lines indicate beam umbra and penumbra determined by target and counter S_3. Dashed lines represent Čerenkov light cone for electron traveling along the axis of the counter.

[15] V. Perez-Mendez and J. M. Pfab, Nucl. Instr. Methods 33, 141 (1965).
[16] V. Perez-Mendez, T. Devlin, J. Solomon, and T. Droege, Nucl. Instr. Methods 46, 197 (1967).
[17] P. Boynton, thesis, Princeton-Pennsylvania Accelerator Internal Report No. PPAD 633 F, 1967 (unpublished).

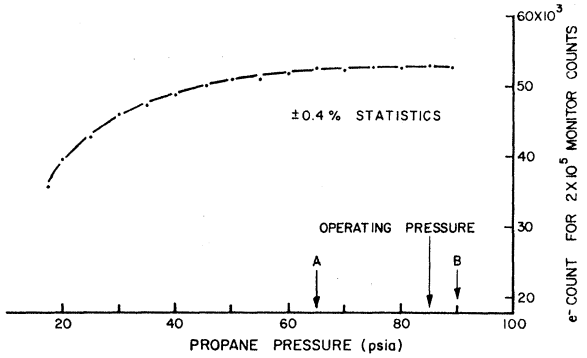

FIG. 6. Electron-count rate as function of Čerenkov radiator pressure. A detection efficiency >98% is implied (see text).

etics pulse amplifier and discriminator. The tube base was similar in design to those mentioned earlier for 56AVP use.

Counter performance was measured by placing the spectrometer–Čerenkov-counter combination directly in a 300-MeV/c negative pion beam (with ~25% electron component) and recording the coincidence ratio $R=BCSS_{4c}/BSS_{4c}$ (see Fig. 2) as a function of gas pressure. The inclusion of S_{4c} in the logic requirement determines that only the 300-MeV/c beam registers in the monitor. The resulting pressure curve is shown in Fig. 6. In order to infer counter efficiency from the plateau characteristic of these data, consideration must be given to two extraneous contributions to the slope of the apparently flat region between A (65 psia) and B (90 psia):

(a) nuclear scattering of π^-, $+3.6\%/(\text{g/cm}^2)$,

(b) electron bremsstrahlung, $-2.2\%/(\text{g/cm}^2)$.

The change in mass between pressures A and B is 0.3 g/cm². Thus from these effects R should increase by 0.4% in that same interval—this amount is within the statistical uncertainty of the data. On the other hand, the index of refraction increases by 40% over the interval AB. From simple arguments involving photoelectron statistics the percentage change in efficiency for a 40% increase in Čerenkov light is roughly equal to the percentage *inefficiency* at point A. From Fig. 6 this change is observed to be 0.8% and is consistent with an efficiency of 99% at point A. We conclude that the electron rejection efficiency can be *conservatively* rated as >98% for operation at 85 psia.

The electron background was measured by observing the Čerenkov-counter *coincidence* rate for experimental conditions otherwise identical to those for recording DCX data on vanadium. After processing the data, two electron events in the momentum range of interest (>210 MeV/c)[17a] were observed in 10^9 monitor counts (2-h run time). In this same period, three DCX events would be expected (cf. Table III), two were actually observed. Thus, with the electron rate roughly equal to the DCX rate for vanadium and with the demonstrated Čerenkov-counter efficiency (greater than 98%), the electron background is less than 2% of the vanadium DCX rate. Background rates for zirconium and lithium targets are easily estimated from the vanadium measurement.[17] The resulting background cross sections for the Čerenkov counter in *anticoincidence* with an efficiency of 98% are reviewed in Table IV. Noted here is the integrated "noise level" from 220 to 320 MeV/c and the background in a 10-MeV bin including the anticipated IAS channel.

TABLE III. Summary of event- and monitor-count data; $T_{\pi^+}=192$ MeV, $110<T_{\pi^-}<210$ MeV. Monitor is defined as the coincidence $B_1B_2B_3$ (see Fig. 2) and is approximately twice the beam on target.

	16°		8.5°	
Target	Event count	Monitor count	Event count	Monitor count
Zr	91	39.1×10^9	77	33.6×10^9
V	130	37.1×10^9	48	13.0×10^9
Li	173	14.9×10^9	···	···
Target out	0	4.65×10^9	4	11.94×10^9

TABLE IV. Electron-background summary for 98% electron rejection efficiency. Values are essentially the same for 8.5° and 16° scattering angles. Uncertainty on each value is +110, −30%.

Element	$(\partial\sigma/\partial\Omega)_{e^-}$ (IAS channel) (μb/sr)	$(\partial\sigma/\partial\Omega)_{e^-}$ (110–210 MeV) (μb/sr)
L	0.005	0.1
V	0.03	0.6
Zr	0.05	1.0

DATA ANALYSIS

The fundamental problem in analysis is the decision whether a given pair of spark-chamber tracks does ("good" event) or does not ("bad" event) correspond to the continuous trajectory of a single particle through the spectrometer. Because of the low DCX reaction rate, a majority (up to 85%) of recorded triggers involved two distinct particles in the two chambers. The situation is made more difficult by the fact that each event must be tagged with a momentum value in order to construct a spectrum. This requirement forces an event-by-event decision of "goodness" which inherently involves greater risk than an ensemble estimate of the proportion of good events. The problem was approached as a hypothesis test on a χ^2 statistic derived from a full five-parameter[18] minimum variance fit of a hypothetical good trajectory to the two-spark chamber tracks. Considerable confidence is gained in each decision by the use of a reduced degree of freedom

[17a] This and all further momentum and energy values refer to conditions immediately prior to the DCX target, not within the C magnet as in the discussion concerning Fig. 3.

[18] The five parameters chosen to uniquely define particle trajectories through the spectrometer are all specified in the target plane: the momentum; x, y position; and two direction cosines.

statistic which may be of some general interest in spark-chamber data analysis. Details of this entire scheme may be found in Ref. 17. Despite the relative strength of these statistical methods, they would be of limited practical value without a large sample of known good events to define quantitatively the distributional properties of the test statistic. Such an ensemble of events was produced by recording elastically scattered π^- under conditions identical to those for the DCX data. The reaction rate was very high relative to DCX scattering and consequently the accidental or two-particle background was negligible. (The value of these scattering data in calibration and testing of many aspects of this experiment cannot be overemphasized.) This "high-purity" sample of good events indicated the general validity of the statistical method, enabled selection of an appropriate significance level for the hypothesis test, and allowed an estimate of the distribution of the test statistic for bad events. Figure 7 indicates the excellent separation typically achieved between good and bad events.

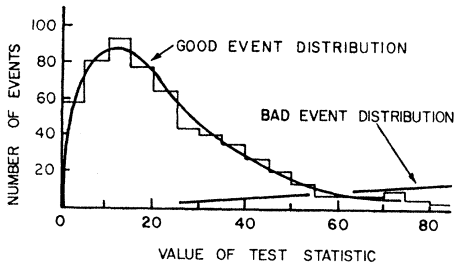

FIG. 7. Curves show approximate distribution of χ^2 statistic for "good" events (from the histogrammed sample of 600 elastic scatters; see text) and for "bad" events (deduced from the 16° zirconium data by subtraction of properly scaled "good" event distribution).

The data analysis also involved corrections for pion energy loss, absorption, and π-μ decay in the spectrometer. Details are discussed in Ref. 17.

RESULTS

Errors quoted in this section are statistical only. They reflect the target-out subtraction and counting statistics. Unless otherwise noted, all uncertainties are expressed as 68% Poisson confidence intervals.

Double Differential Cross Sections

The DCX energy-angular differential cross section $\partial^2\sigma/\partial E\partial\Omega$ for V^{51} and Zr^{90}, evaluated at 8.5° and 16° lab angle, are shown in Figs. 8(a)–8(d). The result for Li^7 is available at 16° lab angle only and is shown in Fig. 8(e). The 8.5° data have been integrated over a solid angle of 3.04 msr which subtends an angular range of 2.15° about the central scattering angle. For the 16° data, the solid angle is 4.05 msr and the angular increment is 2.45°.

TABLE V. Double-change-exchange cross-section summary, $d\sigma/d\Omega$ (110–210 MeV).

Mean scattering angle	$d\sigma/d\Omega$ (μb/sr) Zr	V	Li
8.5°	$49.0_{-6.0}{}^{+7.5}$	$60.2_{-8.9}{}^{+9.2}$	...
16°	$35.0_{-3.9}{}^{+6.0}$	$36.8_{-3.4}{}^{+4.3}$	51.3±3.9

The distributions have been histogrammed in 10-MeV bins. This choice was motivated mainly by the fact that 10 MeV is roughly the incident beam width (FWHM) and thus this bin size optimizes the signal-to-noise ratio for observation of the DCX two-body final state. For the same reason (beam spread), this is nominally the largest bin width that will not appreciably affect the measured shape of the distribution. Both corrected and raw cross sections are displayed.

Single Differential Cross Sections

For the energy interval 110–190 MeV, the angular differential cross sections averaged over the angular extent of S_3 are shown in Table V. These differential cross-section estimates were obtained by summing over the binned energy distributions presented in the previous section. The lowest-energy bin was not included because the variance estimate in that one bin would dominate the error term of the sum.

Two-Body Final State

The cross section upper bounds in Table VI are based on the number of events observed in a 10-MeV interval centered on the two-body final-state energies calculated previously. For comparison, two estimates are given for each set of measurements. The first corresponds to the upper limit of a 68% Poisson confidence interval, the second, a 90% interval. For efficient use of the available information, the data for both scattering angles are combined in the second part of the table. This pooling involves the assumption that the angular distribution falls off by a factor of 2 between 8.5° and 16°.[19]

TABLE VI. Two-body final-state cross-section upper bounds (u.b.) expressed as 68 and 90% Poisson confidence interval (c.i.) upper limits.

Element	Mean scattering angle	Number of events	u.b. for 68% c.i. (μb/sr)	u.b. for 90% c.i. (μb/sr)
Zr	16°	2	1.25	1.70
V	16°	3	1.29	1.67
Zr	8.5°	1	1.54	2.20
V	8.5°	0	1.63	2.70
Pooled estimates				
Zr		3	1.26	1.63
V		3	1.16	1.50

[19] Based on the calculation of Brown and Barshay (Ref. 11) of angular distribution for scattering from $f_{7/2}$ neutrons.

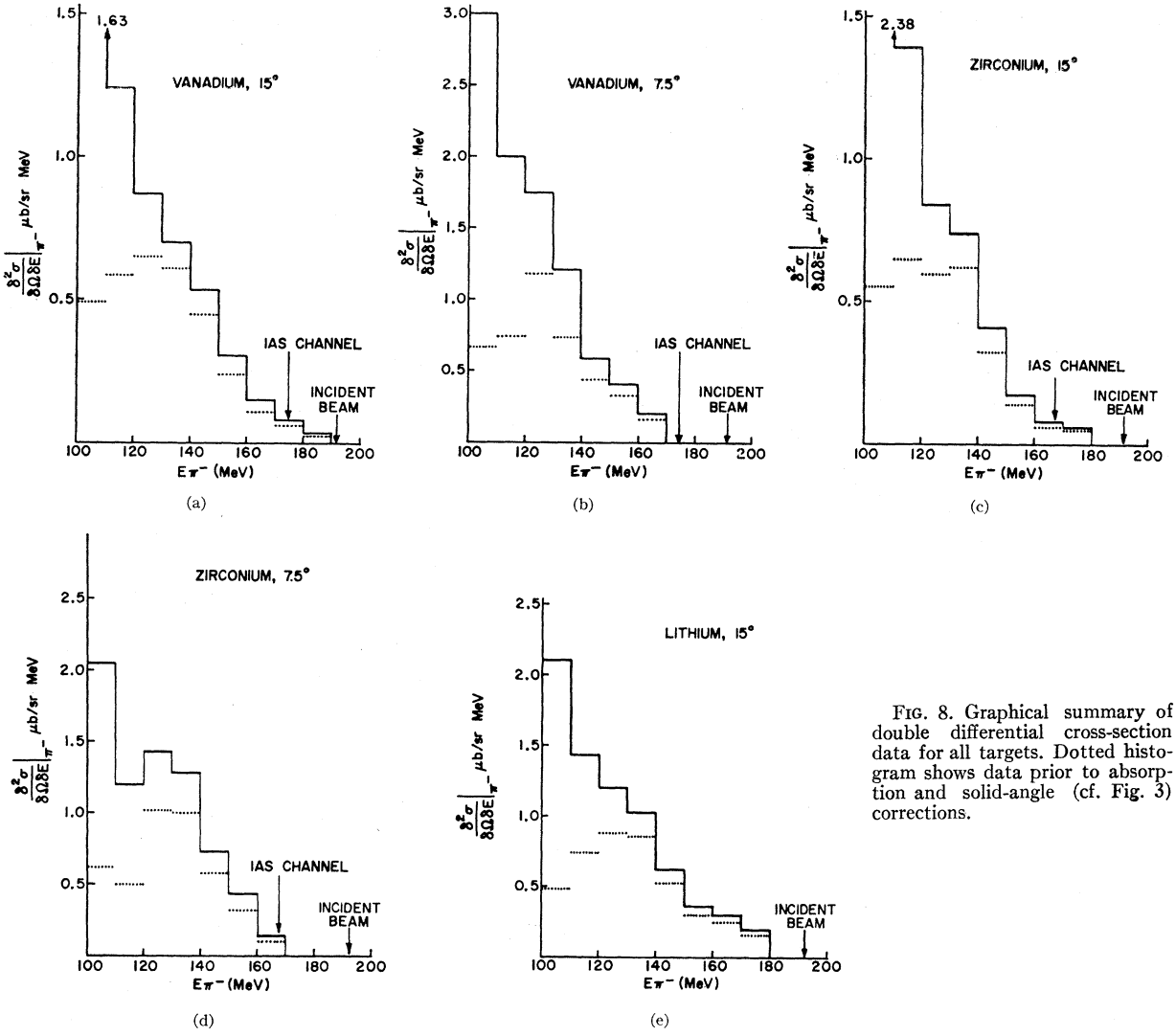

FIG. 8. Graphical summary of double differential cross-section data for all targets. Dotted histogram shows data prior to absorption and solid-angle (cf. Fig. 3) corrections.

DISCUSSION

Review of Data

1. Analog-state excitation. We have no experimental evidence for any two-body final state in vanadium or zirconium. This statement also holds for lithium and is in apparent disagreement with the CERN data.

Figure 9 compares our results for DCX in lithium at 16° lab angle with those of the CERN group at 0°. Their interpretation is that these latter data follow their beam-energy profile displaced to a lower energy and therefore indicate that a considerable fraction of the DCX interaction in Li^7 proceeds through a two-body channel. Our data do not exhibit this energy dependence, and we have no explanation for this observational discrepancy.

It does not appear possible that the disagreement between these data stems from an electron-background problem. The minimal nature of the electron background in our work, less than 2%, was determined by direct measurement. Another indication of low electron contamination is present in the DCX data themselves. The electron background associated with the lithium target should be $<5\%$ of that for zirconium.[17] However, the measured DCX cross section for lithium is 50% greater than for zirconium.

2. Dependence of inelastic cross section on atomic number. The differential cross section at 16° shows a statistically significant decrease for A increasing from 7 (Li) to 51 (V) and no discernible change for 51 (V) compared with 90 (Zr). This same effect—decreasing forward cross section for increasing A—was also observed by the CERN group. Their data show a much stronger dependence, however (see Table VII).

3. Energy dependence of inelastic DCX cross sections. The inelastic π^- energy spectra in Fig. 8 appear essentially as anticipated—beginning with the beam energy

minus the Coulomb and rising sharply for decreasing energy.

4. Angular distribution. The information given in Table V indicates that the differential cross section decreases 20–30% in going from 8.5° to 16°.

Inelastic Pion-Nucleus Scattering

In order to understand these general features of the data and to evaluate the effect of multiple scattering, the following pion-nucleus interaction model was investigated.

Under the combined simplifications of the Born and impulse approximations, the pion-nucleus single-scattering cross section may be written as

$$\frac{d\sigma}{d\Omega} \propto \left(\frac{d\sigma}{d\Omega}\right)_{\text{free}} \sum_{\substack{\text{final}\\ \text{states}}} |\langle f|e^{i\mathbf{q}\cdot\mathbf{r}}|i\rangle|^2,$$

where $(d\sigma/d\Omega)_{\text{free}}$ is the empirical π-N free-particle cross

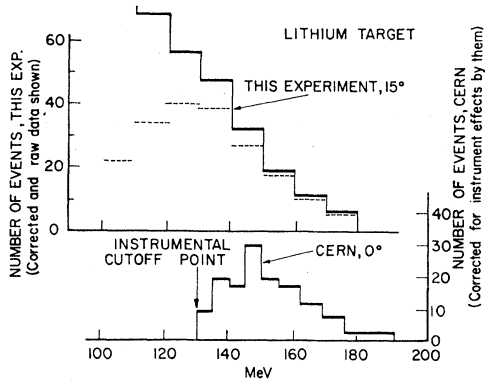

FIG. 9. Comparison of Li^7 data to previous measurement by CERN group (Ref. 7) at 0° scattering angle.

section, and the presence of nuclear matter is expressed through the form-factor term on the right. The latter can be simply evaluated by assuming a Fermi-gas model for the nucleus to specify the distribution of initial states. The sum over final states is then determined by energy-momentum conservation and the exclusion principle. Off-mass-shell scattering is ignored with some justification.[20]

For multiple-scattering problems, this prescription is easily carried out as a Monte Carlo calculation. Such a procedure was first used by Goldberger in early studies of nucleon cascades in complex nuclei.[21] Since that time, the model has enjoyed considerable success in studying nucleon evaporation, yield of spallation products, and the energy and angular distribution of scattered nucleons and pions.[22,23] Recently, the same method

[20] F. Becker and Z. Maric, Nuovo Cimento **39**, 184 (1966).
[21] M. Goldberger, Phys. Rev. **64**, 1268 (1948).
[22] N. Metropolis *et al.*, Phys. Rev. **110**, 185 (1958).
[23] H. Bertini, Phys. Rev. **131**, 1801 (1963).

TABLE VII. Atomic-number dependence of DCX cross sections (in μb/sr). The 0° data are from the CERN experiment (Gilly *et al.*[a]); the 16° data are our own.

	Li	Be	Na	V	Zr
$(d\sigma/d\Omega)_{16°}$	51.3 ± 3.9	...	...	$36.8_{-3.4}^{+4.3}$	$35.0_{-3.9}^{+6.0}$
$(d\sigma/d\Omega)_{0°}$	$90\ \pm1$	10 ± 3	$1.4_{-0.7}^{+1.0}$	...	...

[a] Reference 7.

was used to calculate the excitation function for pion single-charge-exchange scattering in complex nuclei.[24]

The details of the present calculation are similar to those in Refs. 22–24. The free-particle mean free path and angular distributions for charge exchange and elastic scattering were compiled from available π-N cross-section data 50–350 MeV and were used in tabular form in the computation.[25] Also included was attenuation by the two-nucleon absorption process (calculated from pion-deuteron capture cross section).[26] A nuclear radius parameter of 1.3 F was used throughout, along with a nominal neutron Fermi energy of 30 MeV.[22] The reaction was "forced" to proceed through two successive charge-exchange interactions—all further scatters were unrestricted. Each interaction was weighted by the appropriate Clebsch-Gordan coefficients. The calculated differential cross sections shown in Table VIII are found to be a factor of 2–3 higher than the measured values (over the same energy interval and roughly the same angular range). The results for the energy dependence of the differential distribution $\partial^2\sigma/\partial E\partial\Omega$ computed for zirconium are compared with the data on that element in Fig. 10 (the calculated values have been normalized to "fit" the data). Apart from the scale factor, the agreement is quite good compared with that

TABLE VIII. Results of the Monte Carlo multiple-scattering computation for T_π->110 MeV. An order-by-order rescattering count is given in the last column.

Nucleus	$d\sigma/d\Omega$ (10°–20°) (μb/sr)	Rescattering data, 10°–20° Order of scatter	Number of scatters
Li^7	140 ± 16	2	303
		3	166
		4	57
		5	7
V^{51}	94 ± 10	2	210
		3	164
		4	53
		5	11
Zr^{90}	$85\pm\ 9$	2	219
		3	185
		4	68
		5	24

[24] S. Kaufman and C. Hower, Phys. Rev. **140**, B1272 (1965).
[25] V. S. Barashenkov and V. M. Maltsev, Fortschr. Physik **9**, 549 (1961).
[26] R. Frank, J. Gammel, and K. Watson, Phys. Rev. **101**, 891 (1956).

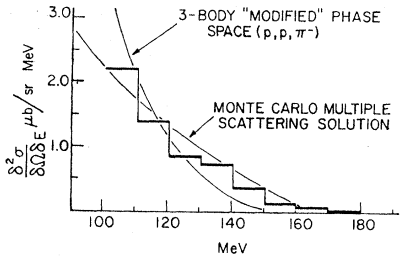

FIG. 10. Comparison of $(\partial^2\sigma/\partial\Omega\partial E)_{16°}$ measured for zirconium (histogram) with Monte Carlo results and three-body phase space which includes effects of nucleon momentum and exclusion principle.

for the three-body phase-space results (p,p,π^-). This latter curve (which has a definite cutoff at 150 MeV) was computed for charge exchange on a neutron pair, again taking the Fermi momentum distribution of the neutrons into account as well as the exclusion principle.

As in previous calculations,[21] the angular distribution shows a minimum in the forward direction due to the inhibiting effect of the exclusion principle on low-momentum-transfer reactions. Because coherent scattering processes were not included, the calculation would not be expected to show a forward-peaked angular dependence.

Higher-Order Scatters

The energy dependence of the differential cross section for the high-energy part of the spectrum (T_π->110 MeV) is sensitive to tertiary and higher-order collisions. The nominal agreement (considering the crudeness of the model) between the computation and experiment lends credibility to the importance of multiple scatters (three and higher) indicated in Table VIII. The relevance of this effect to the observation of IAS is simply that additional scatters tend to destroy the two-body signature of this reaction. Coupled with the pion-absorption mechanism already discussed, the observability of IAS transitions is, however, only moderately restricted. A conservative view of the computation indicates a 10% two-nucleon absorption in addition to a 50% inelastic rescattering probability for 10°–20° scattering in vanadium or zirconium. The observable IAS two-body cross section is thereby depressed by only a factor of 2. The effect is not so pronounced in lithium, but the intrinsic DCX cross section is expected to be much lower [Eq. (2)].

Considering the original estimates of 100–200 μb/sr for the IAS cross section in vanadium and zirconium, depression by a factor of 2 is hardly sufficient to explain the very small (1–2 μb/sr) upper limits placed on the two-body state.

It is apparent that the observability of analog-state transitions at the 3,3 resonance is not significantly restricted by multiple-scattering effects and no advantage is gained in this respect by using a beam energy removed from the 3,3 resonance to avoid the shorter mean free paths for absorption and scattering encountered in the experiment. For 30-MeV incident π^+ kinetic energy the total π-N cross section is down by approximately a factor of 10 and multiple-scattering effects are clearly negligible. Although the elementary-charge-exchange cross section is reduced by a similar factor, that for DCX is not expected to decrease by even an order of magnitude according to the treatment of Koltun and Reitan.[27] Such an experiment was already discussed briefly (Cook *et al.*). Results indicate cross-section upper limits comparable with those in our own experiment.

SUMMARY

The lack of observation of IAS transitions in the DCX data does not appear attributable to inelastic rescattering effects which wash out the two-body signature of this process. We conclude that the cross sections for excitation of these states in vanadium and zirconium are observed to be two orders of magnitude less than currently predicted in the literature.

ACKNOWLEDGMENTS

We wish to thank James Vale and the staff of the 184-in. cyclotron for their valuable assistance. T. Droege, J. Pfab, and H. Johnson were responsible for the detailed design and construction of the wire-spark-chamber system. Dr. Harold Weisburg, Arnold Dicke, Bo Casserberg, and Dr. Leon Kaufman provided valuable assistance in the setup and operation of the experiment. Dr. George Bertsch contributed a number of suggestions about theoretical aspects of this paper. Dr. David Wallace and Gordon Sande made valuable contributions to the statistical analysis. The Princeton group wishes to thank Dr. Milton G. White and the staff of the Princeton-Pennsylvania Accelerator for their support of this work, and the Lawrence Radiation Laboratory for its hospitality. Computer facilities used in the analysis were supported in part by National Science Foundation under Grant No. NSF-GP579.

[27] D. S. Koltun and A. Reitan, Phys. Rev. **139**, B1372 (1965).